DOI https: //doi. org/10.1007/s11595-021-2397-7

Densification and Structure Evolution of ZrB_2-ZrO_2 Composites Prepared by Plasma Activated Sintering using ZrB_2@ZrO_2 Powder

YANG Haitao, ZHANG Jian, LI Junguo*, SHEN Qiang

(State Key Laboratory of Advanced Technology for Materials Synthesis and Processing, Wuhan University of Technology, Wuhan 430070, China)

Abstract: The densification and the structure evolution of the plasma activated sintered (PAS sintered) ZrB_2-ZrO_2 composite via the ZrO_2-coated ZrB_2 powder (ZrB_2@ZrO_2) prepared by in situ passivation method were investigated. The composition and microstructure were characterized by XRD, Raman, SEM, and EDS techniques. The coated powder has excellent sintering performance. The relative density of the composite reaches above 90% at 1 200 ℃, and the main sintering process occurs between ZrO_2 particles. While at above 1 500 ℃, the relative density reaches above 95% and the main sintering process occurs between ZrB_2 and ZrO_2 particles. With the increase of ZrO_2 coating content, the structure of the sintered body changes from ZrB_2 continuous network structure to island structure. When the content is 20%, an island structure is formed. Increasing the ZrO_2 content further causes the overheating of ZrO_2. Thus, the best sintering performance reaches when the coating content is 20wt%.

Key words: ZrB_2; ZrO_2; coating content; densification; structure evolution

1 Introduction

Zirconium diboride (ZrB_2) based composite is attractive for use in ultra-high temperature field due to its unique combination of physical and mechanical properties such as the high melting point and relative low density. However, the low sinterability, low fracture toughness and poor oxidation resistance of the monolithic ZrB_2 limit its wide applications[1-3].

The introduction of second phase, such as SiC[4-6], Si_3N_4[7], ZrC[8], and ZrO_2[9-13], was the common strategy to overcome the above disadvantages. Zhang *et al*[4] prepared ZrB_2-SiC composite by pressureless sintering. It has an excellent oxidation resistance whose mass gain was only 5 mg·cm^{-2} after oxidized at 1 500 ℃ for 30 min. Li *et al*[13] fabricated a series of ZrB_2-ZrO_2 composites by hot pressing. They found that the relative density of the composite increase with the ZrO_2 content. ZrB_2-30vol% ZrO_2 composite provided the optimal combination of dense microstructure, high hardness of 22.7 GPa and high fracture toughness of 6.5 MPa·m$^{1/2}$.

The introduction of a second phase as a powder coating, especially for the nanoscale one, contributes to improving the mixing uniformity of each phase and optimizing the structure of composite, thus further improving the performance. Ang *et al*[14] prepared the ZrB_2@(ZrO_2/C) composite powder using sol-gel method. The ZrO_2/C coating reacted to produce the nanoscale ZrC during the sintering process, promoted the densification and inhibited the grain growth. Guo *et al*[15] fabricated the ZrB_2@(Zr/Al) composite powders using ball milling process. Then the ball milled powers were mixed with graphite powders and SiC powders and sintered to prepare the ZrB_2-SiC-ZrAlC composite ceramics. The Zr/Al coating reacted with graphite to in situ produce layered ZrAlC compound. A more uniform microstructure of the ceramic was obtained than that of the ceramic using the un-milled powder, thus gained a high toughness of 5.96 MPa·m$^{1/2}$. Song *et al*[12,16] successfully prepared the ZrB_2@ZrO_2 composite powder by co-precipitation method. The composite powder was found to promote the densification compared with that of uncoated one. The relative density of the Zr-

(Received: May 21, 2020; Accepted: Aug. 18, 2020)

YANG Haitao(杨海涛): Ph D; E-mail: Haitaoyang_2013@163.com

*Corresponding author: LI Junguo(李俊国): Prof.; Ph D; E-mail:lijg000@126.com

Funded by the National Natural Science Fund of China (Nos.51272190, 51521001), the 111 Project of China (B13035), the Major Projects of Technological Innovation of Hubei Province (2019AFA176) and the National Key Research and Development Program of China (2017YFB0310400)

B_2@10wt% ZrO_2 composite ceramic reached 95% after sintered at 1 900 ℃. The thermal shock resistance and the oxidation resistance were also improved.

However, the coating quality of the above composite powders is not satisfying. The various coatings prepared by the sol-gel, ball-milling, and the co-precipitation methods have incomplete coverage and the thicknesses are not uniform. The composite powder with a high coating quality would further optimize the structure of the composites. In our previous work[17], the ZrB_2@ZrO_2 composite powder with uniform thickness, full coverage and controllable coating content was prepared by in situ passivation reaction. The passivation reaction transformed the surface of ZrB_2 powder to the ZrO_2 coating. The coating content was controllable by adjusting reaction time.

Based on these, a series of ZrB_2@ZrO_2 composite powders prepared by in situ passivation reaction were used here. Then the densification behavior of the coated powders was studied. And the influence of coating content on sintering properties, structural evolution and mechanical properties of the ZrB_2@ZrO_2 composite materials would be further analyzed.

2 Experimental

2.1 Synthesis of the coated powders

As-received ZrB_2 powder shown in Fig.1(a) with an average size 10-15 μm and clean surface was provided by Qinhuangdao ENO High-Tech Material Development Co., Ltd. in China. The mixture of NaOH and H_2O_2 solution (total volume, 60 mL) was filled in a 100 mL Teflon liner at room temperature. The NaOH and H_2O_2 concentration were 1 mol·L^{-1} and 2 mol·L^{-1}, respectively. Then a Teflon tube loaded with 2 g ZrB_2 powders was transferred into the Teflon liner. The Teflon liner was placed in an autoclave and preheated at 140 ℃ for 4 h. After preheated, the autoclave was taken out and inversed for several times to keep the sufficient contact between the powder and the mixed solution, and then moved back to the furnace for several hours (2-24 h). The coating content was controlled by the reaction time. After cooling to room temperature, the mixture was transferred from the Teflon liner to a beaker that filled with 3 000 mL water. After standing for 30 min, the liquid supernatant and the solid product were separated. The collected solid product was then rinsed with deionized water and ethanol for five times, and finally dried at 80 ℃ for 24 h.

2.2 PAS sintering

The coated powders and the uncoated powders with the same composition were loaded into cylindrical graphite (inner diameter, 20 mm) dies that lined with flexible graphite foils. The sintering process was conducted by the plasma activated sintering equipment (PAS, ED-PAS 111 equipment, Elenix, Zama Shi, Japan) at different sintering temperatures for 10 min under a uniaxial load of 40 MPa in Ar atmosphere with a sintering speed of 100 ℃·min^{-1}.

2.3 Characterizations

The compositions of the coated powder and the sintered composites were analyzed by X-ray diffraction (XRD, RU-200B/D/MAX-RB, Rigaku Corporation, Japan) using Cu Kα1 radiation and Raman spectra (LabRAM HR800, Horiba, USA) using the 325 nm laser excitation. The scanning range of XRD is 25°-45° and the scanning speed is 4 °·min^{-1}. The Raman spectra were recorded in the range of 50-700 cm^{-1}. The whole coating content was calculated by the RIR method using the XRD results of the sintered composite. The morphology of the coated powder and the microstructure of the composites were characterized by the field emission scanning electron microscopy (FE-SEM, Quanta 250, FEI, USA) equipped with the energy dispersive X-ray spectroscopy (EDS, 51-XMX1005, Oxford Instruments Inc., UK). The density of the sintered composites was measured by Archimedes principle. The volume electrical resistivity of the composites was tested by four-point probe method using the Hall measurement system (H-50, MMR Technologies Inc.). The hardness of the composites was tested by Vickers hardness tester (Wolpert 430SV, Wolpert Wilson Instruments, Aachen, Germany) with a load of 3 kg for 15 s. Fracture toughness (K_{IC}) was evaluated by a single-edge notched-beam test with a 16-mm span and a crosshead speed of 0.05 mm·min^{-1} using 2 mm×4 mm×20 mm test bars on a hydraulic universal testing machine (Instron 5966, UK). The mechanical tests were repeated five times.

3 Results and discussion

3.1 Characterization of the coated powder

The morphology of the coated powder with the reaction time of 24 h is shown in Fig.1(b). Different from the smooth and clean surface of the raw ZrB_2 powder (Fig.1(a)), the surface of the coated powder exhibits a large amount of homogeneously distributed short rode-like crystals with sub-micron scale size. And the

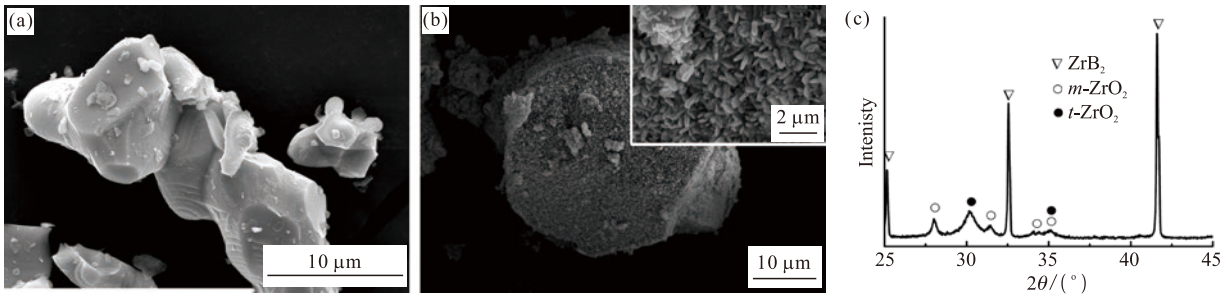

Fig.1 The morphologies of raw ZrB_2 powder(a) and ZrB_2@ZrO_2 powder(b) with the reaction time of 24 h; (c) XRD pattern of ZrB_2@ZrO_2 powder

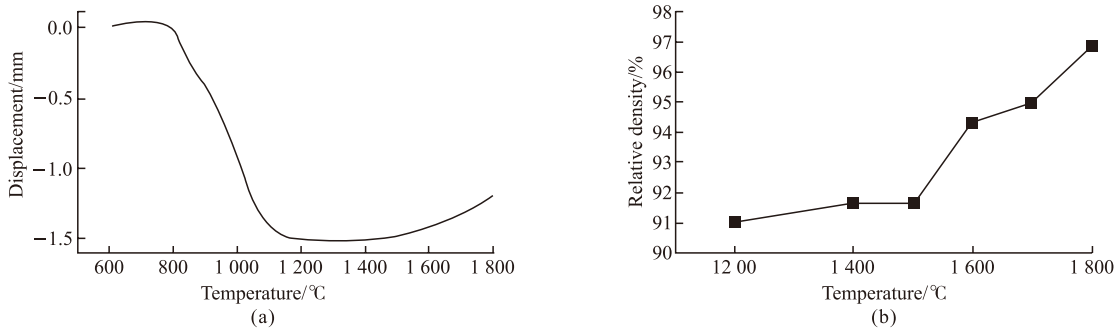

Fig.2 (a) Shrinkage curve of the ZrB_2@ZrO_2 composite using the coated powder with the reaction time of 24 h; (b) Relative densities of the composite at different sintering temperatures for 10 min under a pressure of 40 MPa

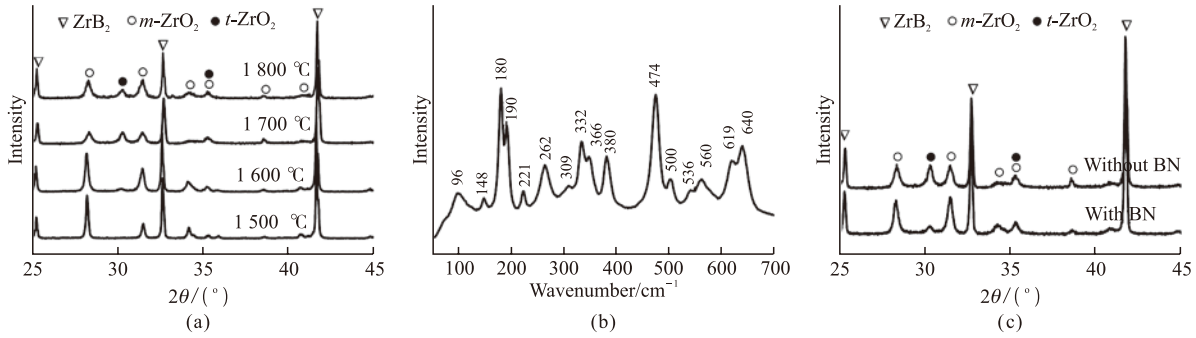

Fig.3 (a) XRD patterns of the ZrB_2@ZrO_2 composites sintered at different temperatures using the coated powder with the reaction time of 24 h. The ZrO_2 coating content is calculated to be about 30wt% by the RIR method; (b) Raman spectrum of the coated composite sintered at 1 700 ℃; (c) XRD patterns of the coated composites sintered at 1 700 ℃ with and without the BN segregation during sintering

coverage of the coating approaches 100%. The phase analysis in Fig.1(c) shows that the product is composed of monoclinic zirconia (*m*-ZrO_2), tetragonal zirconia (*t*-ZrO_2), and ZrB_2 phase.

3.2 Effect of temperature on densification behabior

3.2.1 Shrinkage and relative density

Fig.2(a) shows the shrinkage curve of the ZrB_2@ZrO_2 composite using the coated powder with the reaction time of 24 h. As can be seen, the volume shrinkage is not apparent when the temperature is below 800 ℃. The shirinkage starts at 8 00-1 200 ℃, which corresponds to the sharp contraction of ZrO_2 in this temperature range[18]. The shrinkage ends at 1 200-1 500 ℃. At temperatures above 1 500 ℃, the volume expands slightly.

Fig.2(b) shows the relative densities of the ZrB_2@ZrO_2 composite sintered at different temperatures. When calculating the relative density, the theoretical density is obtained by the mixing rules using the content of the composition derived from the RIR results of Fig.3(a). The relative density is 91%-92% and changes little when the temperature is 1 200-1 500 ℃. With the temperature rises, the relative density increases significantly, reaching 95% at 1 700 ℃.

3.2.2 Phase and composition

Fig.3 exhibits the phase and composition analysis of the ZrB_2@ZrO_2 composites. Fig.3(a) is the XRD results of the coated composite sintered at different temperatures. The main phases are ZrB_2 and *m*-ZrO_2. When

the sintering temperature is above 1 600 ℃, there exists a small amount of *t*-ZrO_2 evidenced by the Raman spectrum (Fig.3(b)). The Raman spectrum contains the strong characteristic peaks of *m*-ZrO_2 and the weak characteristic peaks of *t*-ZrO_2(148 and 221 cm^{-1})[19]. The ZrO_2 coating content is calculated to be about 30wt% by the RIR method.

The content of *t*-ZrO_2 is related to the diffusion and doping of carbon element derived from the graphite die during sintering[20]. The higher the sintering temperature, the more the carbon element introduces into the sample which results in the obvious inhibition of martensitic transformation of ZrO_2. Thus, the content of *t*-ZrO_2 increases with the sintering temperature. When the contacts between the coated powders and graphite die is prohibited by the BN spraying, the content of *t*-ZrO_2 is significantly decreased as shown in Fig.3(c).

3.2.3 Microstructures of the coated composites

Fig.4 exhibits the fracture morphologies of the ZrB_2@ZrO_2 composites with 30wt% ZrO_2 sintered at different temperatures. When the sintering temperature is 1 200-1 600 ℃, the ZrB_2 particle shows an island distribution and ZrO_2 particle is a continuous network structure. The ZrO_2 particle grows from sub-micron scale to several microns with the increased sintering temperature. With the further increase of temperature (above 1 600 ℃), the characteristic of the small ZrO_2 particles disappears. The ZrO_2 grain coarsening behavior is apparent.

Fig.5 shows the polished surface of the ZrB_2@ZrO_2 composites with 30wt% ZrO_2 sintered at different temperatures. When the temperature is below 1 600 ℃, the surface exhibits obvious isolated ZrB_2 particles and the porous continuous ZrO_2 particles (Figs.5(a) and

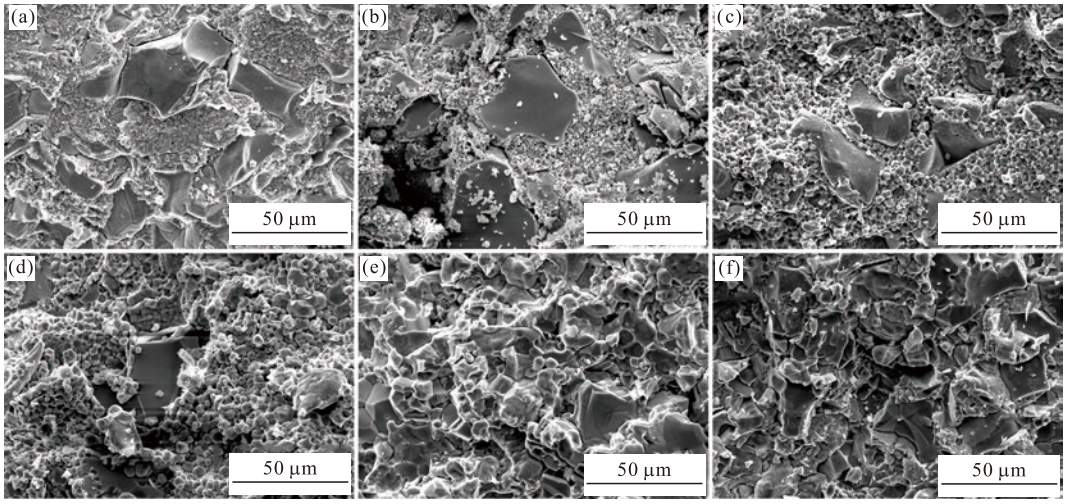

Fig.4 Fracture morphologies of the ZrB_2@ZrO_2 composites with 30wt% ZrO_2 sintered at (a)1 200, (b)1 400, (c)1 500, (d)1 600, (e)1 700, and (f)1 800 ℃ for 10 min

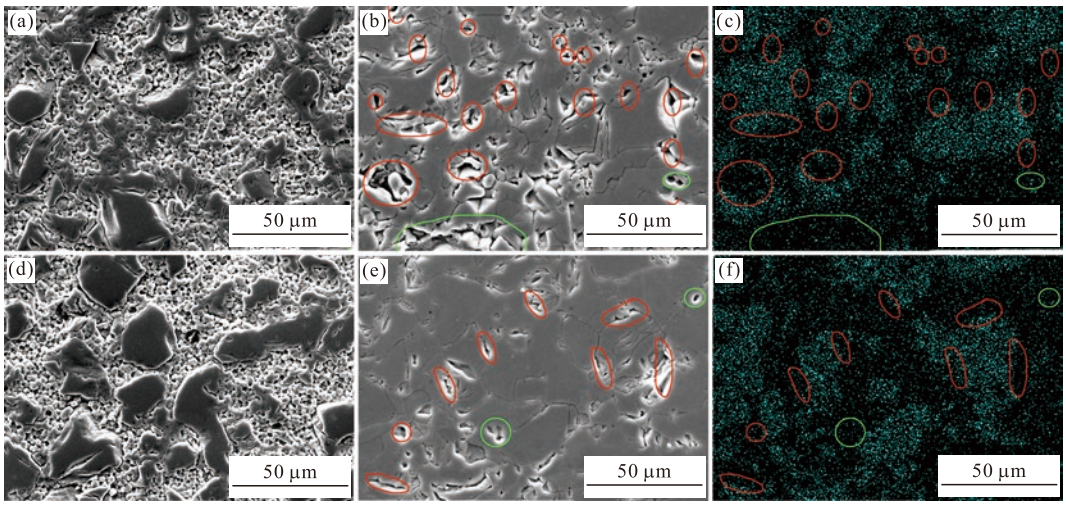

Fig.5 Polished surfaces of the ZrB_2@ZrO_2 composites with 30wt% ZrO_2 sintered at (a)1 500, (d) 1 600, (b) 1 700, and (e) 1 800 ℃, where (c) and (f) correspond to the element B distributions of (b) and (e). The red circle is the pore near the B-enriched zone, and the green circle is the pore away from the B area

5(d)), which is consistent with the fracture morphologies (Fig.4). When the temperature is 1 700-1 800 ℃ (Figs.5(b) and 5(e)), the continuous ZrO_2 particles transform into a whole and the characteristic of small ZrO_2 particles disappears. The ZrB_2 still shows an island distribution from the corresponding EDS maps of B element (Figs.5(c) and 5(f)). There exists large amount of pores between ZrB_2 and ZrO_2 (the red circle) and a few pores between ZrO_2 and ZrO_2 particles (the green circle) when sintered at 1 700 ℃ (Fig.5(b)). The pores between ZrO_2 and ZrO_2 particles results from the oversintering of the ZrO_2 [21, 22] at such high temperature. While at 1 800 ℃, the number of pores between ZrB_2 and ZrO_2 decreases and the pores between ZrO_2 and ZrO_2 particles still remains.

3.3 Effect of coating content on densification behavior

3.3.1 XRD analysis of ZrB_2@ZrO_2 composite

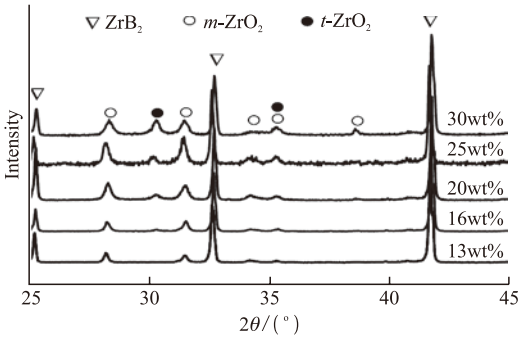

Fig.6 XRD patterns of the ZrB_2@ZrO_2 composites sintered at 1700 ℃ with the reaction time of 2, 4, 8, 12, and 24 h. The corresponding ZrO_2 contents were calculated to be 13wt%, 16wt%, 20wt%, 25wt%, and 30wt%, respectively

Fig.6 shows the XRD patterns of the ZrB_2@ZrO_2 composites sintered at 1 700 ℃ via the coated powders with different reaction time. The phases include ZrB_2, *m*-ZrO_2 and a small amount of *t*-ZrO_2. The whole ZrO_2 content is calculated to be 13wt%-30wt% according to the RIR method. And both the *m*-ZrO_2 and *t*-ZrO_2 gradually increase with the whole coating content.

3.3.2 Relative density of ZrB_2@ZrO_2 composite

Fig.7 shows the relative densities of of the ZrB_2@ZrO_2 composites with various ZrO_2 content sintered at 1 700 ℃. For comparison, the relative densities of uncoated ones are listed. As can be seen, the RD of the coated samples is above 90%, while that of uncoated ones is below 80%. Such results highlight the excellent sintering performance of coated powder. With the increased ZrO_2 content, the RD of the coated samples firstly increases and then decreases. The maximum value of RD reaches about 97% when the ZrO_2 content is 20wt%-25wt%.

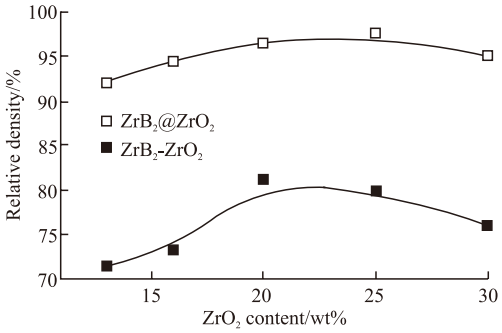

Fig.7 The relative density of of the ZrB_2@ZrO_2 composites with various ZrO_2 content, sintered at 1 700 ℃ for 10 min under a pressure of 40 MPa. The uncoated ones are listed for comparison

3.3.3 Microstruce of ZrB_2@ZrO_2 composite

Fig.8 shows the fracture morphologies of the ZrB_2@ZrO_2 composites with different ZrO_2 contents

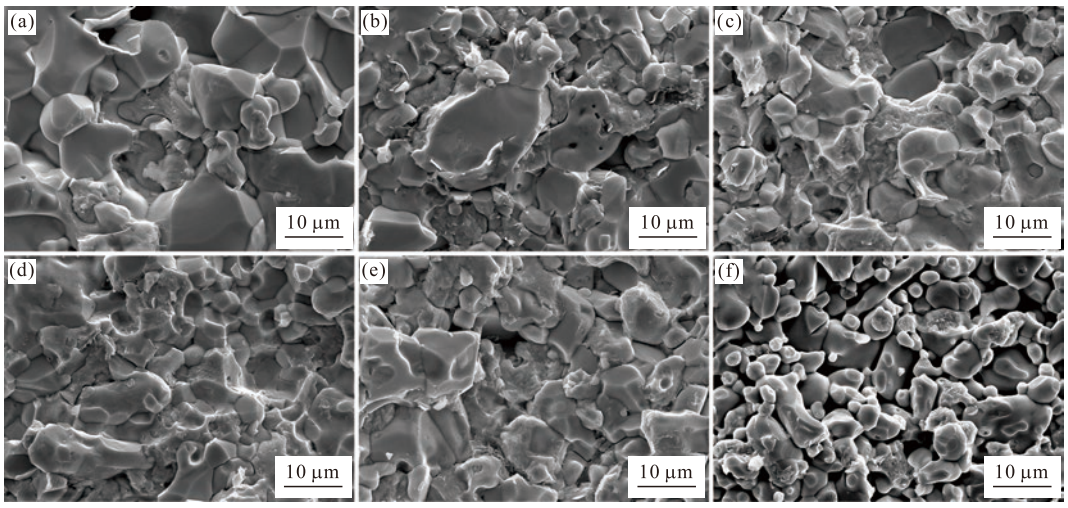

Fig.8 Fracture surfaces of the ZrB_2@ZrO_2 composites with (a) 13wt%, (b) 16wt%, (c) 20wt%, (d) 25wt%, (e) 30wt% ZrO_2 sintered at 1 700 ℃ for 10 min under a pressure of 40 MPa. The uncoated one (f) with 30wt% ZrO_2 is listed for comparison

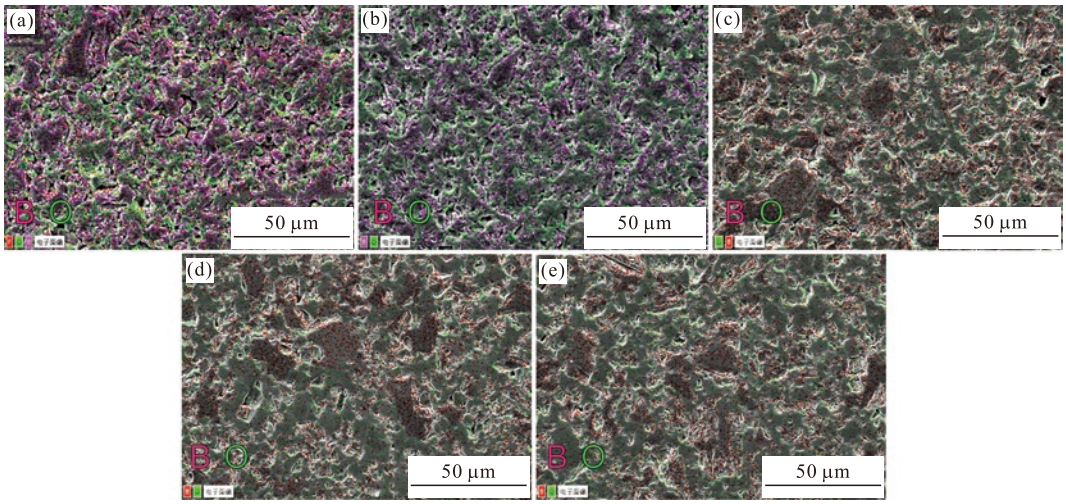

Fig.9 EDS maps for the ZrB_2@ZrO_2 composites with (a) 13wt%, (b) 16wt%, (c) 20wt%, (d) 25wt%, and (e) 30wt% ZrO_2 sintered at 1 700 ℃ where the pink is the element B and the green is the element O

sintered at 1 700 ℃. Compared with the porous microstructure of the uncoated sample (Fig.8(f)), the coated samples show the dense structure. The transgranular fracture and intergranular fracture exist simultaneously. The ZrO_2 enriched areas with irregular shape mainly shows the intergranular fracture.

Fig.9 shows the EDS maps of the polished surface of ZrB_2@ZrO_2 composites with different ZrO_2 contents sintered at 1 700 ℃. The pink is the element B represented the ZrB_2 and the green is the element O represented the ZrO_2. When the ZrO_2 content is 13wt%, the ZrB_2 has a continuous distribution. When the ZrO_2 content is 16wt%, the pink area (ZrB_2) decreases and the continuous network structure remains. However, when the ZrO_2 content rises to 20wt%, the network structure of ZrB_2 is replaced with an island structure. With the further increased ZrO_2 content, the structure changes little.

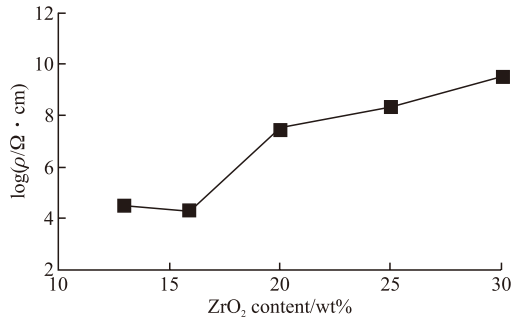

Fig.10 Volume electrical resistivities of the ZrB_2@ZrO_2 composites with various ZrO_2 contents sintered at 1 700 ℃

Fig.10 shows the volume electrical resistivity of the ZrB_2@ZrO_2 composites with various ZrO_2 contents sintered at 1 700 ℃. As can be seen, the resistivity is lower than 10^5 Ω cm when the ZrO_2 content is 13wt%-16wt%. When coated with 20wt% ZrO_2, the resistivity increases sharply to 10^8 Ω·cm. With further increase of ZrO_2 content, the volume resistivity increased slowly. The phenomenon of resistivity mutating at a critical content is its percolation behavior. It reflects the evolution of the three-dimensional conductive network (ZrB_2) from connection to interrupt in the structure. The result is consistent with the analysis of EDS maps (Fig.9). The minimum coating content for the interrupted network structure of ZrB_2 and the formation of the island structure of ZrO_2 is 20wt%.

3.4 Densification mechanism

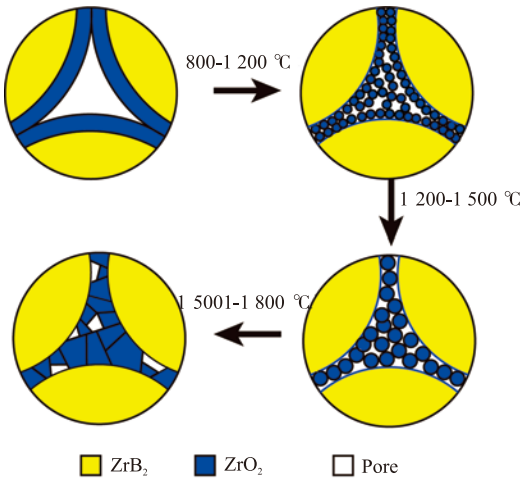

Fig.11 Schematic diagram for the densification mechanism of the ZrB_2@ZrO_2 composites

According to the analysis of the shrinkage curve and the evolution of microstructure of the ZrB_2@ZrO_2 composite, the schematic diagram of the densi-

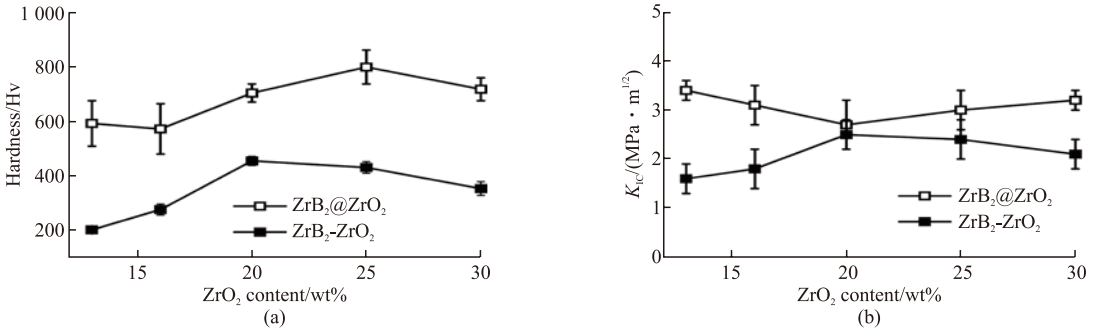

Fig.12 Hardness(a) and Fracture toughness(b) of the ZrB_2@ZrO_2 composites with various ZrO_2 contents sintered at 1 700 ℃. The uncoated ones are listed for comparison

fication mechanism is shown in Fig.11. The sintering process can be divided into four stages: (I) When the temperature rises to 800 ℃, the powder coating gradually dehydrates and crystallizes. The rearrangement starts among the ZrO_2 particles and ZrB_2 particles. (II) When the temperature is 800-1 200 ℃, most of the volume shrinkage is completed and the RD reaches above 90%. The main processes include the enrichment and sintering of the ZrO_2 particles in the boundary and triangular regions between the micron ZrB_2 particles under high temperature and mechanical pressure. The sub-micron scale ZrO_2 makes it high surface activity and contributes to the formation and expansion of the sintering neck of ZrO_2 grains. It corresponds to the sharp shrinkage of ZrO_2 in this temperature range[18]. (III) When the temperature is 1 200-1 500 ℃, the RD changes little. The main sintering process is the slow grain growth of ZrO_2. (IV) When the temperature is above 1 500 ℃, the main sintering process occurs between ZrB_2 and ZrO_2 particles. The RD reaches above 95%. Meanwhile, the ZrO_2 particle coarsening from several microns to 10 microns or more occurs, which corresponds to the oversintering of ZrO_2[21,22] at this high temperature.

The in-situ formed coating of the powder hinders the direct contacts of micron ZrB_2 particles which is difficult to be sintered. The isolation effect of the coating changes the main sintering process. It is transformed into the sintering of the ZrO_2 coating, followed by sintering between ZrB_2 and ZrO_2. The former could be completed below 1 500 ℃ due to its high sintering activity, and the latter needs even high sintering temperature.

When the ZrO_2 coating content is below 20wt%, the dehydration and shrinkage of the coating lead to the incomplete coverage of ZrB_2 powder. There exists a small amount of direct contacts of ZrB_2 particles, which slightly increases the sintering difficulty and forms the network structure of ZrB_2. The direct contact area is much smaller than that of the uncoated sample, resulting in a high RD (>90%). With the increase of ZrO_2 content, the direct contact area of ZrB_2 decreases gradually, and the isolation effect of coating layer is enhanced. Thus, the sintering difficulty is reduced. When the sintering content is 20wt%, the direct contact area of zirconium boride is minimized. And the maximum isolation effect of the coating reaches. Further increasing the coating content, the negative effects of zirconia in oversintering state on densification should not be ignored. As a whole, the ZrB_2@ZrO_2 powder with 20wt% ZrO_2 has the best sintering performance.

3.5 Mechanical properties

Fig.12(a) shows the Vickers hardness of the ZrB_2@ZrO_2 composites with various ZrO_2 content sintered at 1 700 ℃. The uncoated samples are listed for comparison. As can be seen, the Vickers hardness is 600-800 HV. It increases first and then decrease with the increase of coating content, which is similar to the trend of the RD (Fig.7). Both the coated and uncoated samples do not achieve the full density. The porosity, as the third phase, is the most important factor affecting the hardness of composites. Thus, the uncoated composite with high porosity shows an even poor hardness and the trend is similar.

Fig.12(b) shows the fracture toughness (K_{IC}) of the above samples. It changes little with the content. The K_{IC} value is 2.5-3.5 MPa·$m^{1/2}$, slightly higher than that of pure ZrB_2 ceramics (about 2.4 MPa·$m^{1/2}$)[23]. However, compared with the uncoated samples, the K_{IC} of the coated samples is significantly improved. This indicates that the dense structure contributes to improving the fracture toughness of the composite.

4 Conclusions

The ZrB_2@ZrO_2 powders with full coverage and controllable coating content prepared by in-situ passivation reaction have excellent sintering performance. The relative density could reach 95% when sintered at 1 700 ℃.

With the increase of ZrO_2 coating content, the structure of the sintered body changes from ZrB_2 continuous network structure to island structure. When the content is 20%, an island structure is formed. Increasing the ZrO_2 content further causes the overheating of ZrO_2. Thus, the best sintering performance reaches when the coating content is 20wt%.

References

[1] Fahrenholtz WG, Hilmas GE, Talmy IG, *et al*. Refractory Diborides of Zirconium and Hafnium[J]. *J. Am. Ceram. Soc.*, 2007, 90: 1 347-1 364

[2] Guo Q, da Silva CVJ, Bourgeois BB, *et al*. Influence of In-situ Synthesized Zr-Al-C on Microstructure and Toughening of ZrB_2-SiC Composite Ceramics Fabricated by Spark Plasma Sintering[J]. *Ceram. Int.*, 2017, 43: 13 047-13 054

[3] Yuan HP, Li JG, Shen Q, *et al*. Preparation and Microstructure of Porous ZrB_2 Ceramics using Reactive Spark Plasma Sintering Method[J]. *J. Wuhan. Univ. Technol.*, 2015, 30: 512-515

[4] Zhang H, Yan YJ, Huang ZR, *et al*. Properties of ZrB_2-SiC Ceramics by Pressureless Sintering[J]. *J. Am. Ceram. Soc.*, 2009, 92: 1 599-1 602

[5] Shugart K, Liu S, Craven F, *et al*. Determination of Retained B_2O_3 Content in ZrB_2-30vol% SiC Oxide Scales[J]. *J. Am. Ceram. Soc.*, 2015, 98: 287-295

[6] Thimmappa SK, Golla BR, Prasad VB, *et al*. Phase Stability, Hardness and Oxidation Behaviour of Spark Plasma Sintered ZrB_2-SiC-Si_3N_4 Composites[J]. *Ceram. Int.*, 2019, 45: 9 061-9 073

[7] Monteverde F, Bellosi A. Effect of the Addition of Silicon Nitride on Sintering Behaviour and Microstructure of Zirconium Diboride[J]. *Scripta Mater*, 2002, 46: 223-228

[8] Wu WW, Zhang GJ, Kan YM, *et al*. Reactive Hot Pressing of ZrB_2-SiC-ZrC Ultra High-temperature Ceramics at 1 800 ℃[J]. *J. Am. Ceram. Soc.*, 2006, 89: 2 967-2 969

[9] Vafa NP, Nayebi B, Asl MS, *et al*. Reactive Hot Pressing of ZrB_2-based Composites with Changes in ZrO_2/SiC Ratio and Sintering Conditions. Part II: Mechanical Behavior[J]. *Ceram. Int.*, 2016, 42: 2 724-2 733

[10] Zamora V, Ortiz AL, Guiberteau F, *et al*. In situ Formation of ZrB_2-ZrO_2 Ultra-high-temperature Ceramic Composites from High-energy Ball-milled ZrB_2 Powders[J]. *J. Alloy. Comp.*, 2012, 518: 38-43

[11] Zhu T, Li W, Zhang X, *et al*. Damage Tolerance and R-curve Behavior of ZrB_2-ZrO_2 Composites[J]. *Mat. Sci. Eng. A-Struct.*, 2009, 516: 297-301

[12] Song J, Li JG, Shen Q, *et al*. Thermal Shock and Oxidation Resistances of ZrB_2-ZrO_2 Ceramics[J]. *J. Chin. Silicate. Soc.*, 2008, 36: 663-667

[13] Li WJ, Zhang XH, Hong CQ, *et al*. Preparation, Microstructure and Mechanical Properties of ZrB_2-ZrO_2 Ceramics[J]. *J. Eur. Ceram. Soc.*, 2009, 29: 779-786

[14] Ang C, Seeber A, Williams T, *et al*. SPS Densification and Microstructure of ZrB_2 Composites Derived from Sol-Gel ZrC Coating[J]. *J. Eur. Ceram. Soc.*, 2014, 34: 2 875-2 883

[15] Guo QL, Luo SJ, Gan JZ, *et al*. Effect of Ball Milled Zr/Al/ZrB_2 Composite Powders on Microstructure and Toughening of ZrB_2-SiC/Zr-Al-C Composite Ceramics Sintered by Spark Plasma Sintering[J]. *Mat. Sci. Eng. A-Struct.*, 2015, 644: 96-104

[16] Song JR, Shen QA, Li JG, *et al*. Preparation and Characterization of the Coated ZrB_2@ZrO_2 Ceramic[J]. *Adv. Mater. Res.*, 2009, 66: 226-229

[17] Yang H, Zhang J, Li J, *et al*. In-situ Passivation Reaction for Synthesis of a Uniform ZrO_2-coated ZrB_2 Powder in Alkaline Hydrothermal Solution[J]. *Surf. Coat. Technol.*, 2020, 385: 125 385

[18] Tatarko P, Grasso S, Chlup Z, *et al*. Toughening Effect of Multi-Walled Boron Nitride Nanotubes and Their Influence on the Sintering Behaviour of 3Y-TZP Zirconia Ceramics[J]. *J. Eur. Ceram. Soc.*, 2014, 34: 1 829-1 843

[19] Li MJ, Feng ZC, Ying PL, *et al*. Phase Transformation in the Surface Region of Zirconia and Doped Zirconia Detected by UV Raman Spectroscopy[J]. *Phys. Chem. Chem. Phys.*, 2003, 5: 5 326-5 332

[20] Wang D, Liang K, Wan J. Carbon-containg Zirconia Ceramics[J]. *J. Chin. Ceram. Soc.*, 1998, 26: 233-239

[21] Boutz MMR, Winnubst AJA, Hartgers F, *et al*. Effect of Additives on Densification and Deformation of Tetragonal Zirconia[J]. *J. Mater. Sci.*, 1994, 29: 5 374-5 382

[22] Chen F, Jin D, Tyeb K, *et al*. Field Assisted Sintering of Graphene Reinforced Zirconia Ceramics[J]. *Ceram. Int.*, 2015, 41: 6 113-6 116

[23] Monteverde F, Guicciardi S, Bellosi A. Advances in Microstructure and Mechanical Properties of Zirconium Diboride based Ceramics[J]. *Mat. Sci. Eng. A-Struct.*, 2003, 346: 310-319